Volume 6
Number 17
7 September 2024
Pages 4263–4494

Nanoscale Advances

rsc.li/nanoscale-advances

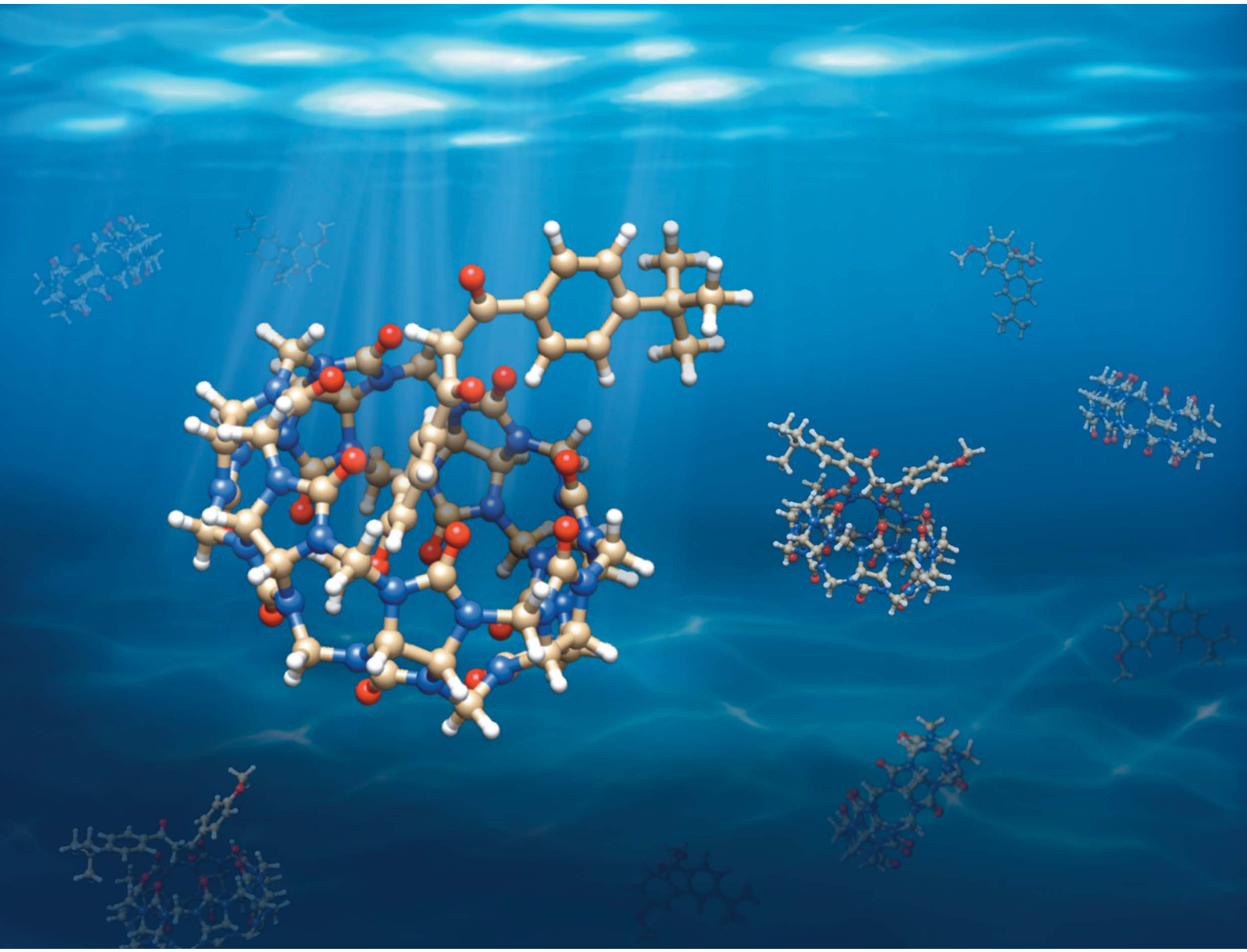

ISSN 2516-0230

ROYAL SOCIETY OF CHEMISTRY

PAPER
Harshita Kumari *et al.*
Dynamic macromolecular material design: the versatility of cucurbituril over cyclodextrin in host–guest chemistry

NCNST

Nanoscale Advances

ROYAL SOCIETY OF CHEMISTRY

PAPER

View Article Online
View Journal | View Issue

Cite this: *Nanoscale Adv.*, 2024, **6**, 4376

Dynamic macromolecular material design: the versatility of cucurbituril over cyclodextrin in host–guest chemistry†

Jinnipha Pajoubpong,[a] Collin M. Mayhan,‡[ab] Ajaz Ahmad Dar,‡[a] Alexander I. Greenwood,[c] Karoline C. Klebba,[b] Matthew L. Cremer[b] and Harshita Kumari *[a]

The keto–enol tautomerism of avobenzone (AVO) is pivotal to its photostability, influenced by microenvironmental factors, such as, the type of solvent and complexation with macrocyclic compounds. This study explores the effect of host–guest complexation on AVO photostabilization, employing cucurbit[7]uril (CB[7]) and β-cyclodextrin (β-CD) to form inclusion complexes. CB[7] exhibits a higher affinity to the keto form of AVO, a UVC radiation absorber. The complexed keto form facilitates the regeneration of the enol form, reducing skin permeation. Spectroscopic and thermal analyses confirm 1 : 1 AVO–CB[7] and AVO–β-CD complex formation. Computational and MD simulations show that host–guest complex is favored over isolated AVO and β-CD or CB[7] molecules by 95–125 kJ mol^{-1}, depending on the presence of implicit solvent. Both macrocycles enhance AVO photostabilization in aqueous environments, with CB[7] displaying greater selectivity for the keto form, while β-CD shows ethanol concentration-dependent binding.

Received 17th April 2024
Accepted 26th June 2024

DOI: 10.1039/d4na00324a

rsc.li/nanoscale-advances

Introduction

Avobenzone (AVO) is a dibenzoylmethane derivative that absorbs the full UVA spectrum (320–400 nm) and has a relatively high molar absorption coefficient (33 756 L (mol cm)$^{-1}$ at 360 nm),[1] resulting in a high UV absorbance efficiency. Consequently, it is the most common active ingredient in chemical sunscreen formulations and has been approved for use globally (up to 3% in the USA and Canada; up to 5% in the EU, UK, and Australia; up to 10% in Japan). However, AVO exhibits poor photostability because it undergoes keto–enol tautomerization upon exposure to light. The enol tautomer, which predominates in solution, absorbs UVA radiation and transforms into the keto form. Notably, the keto form absorbs UVC instead of UVA radiation. The singlet-excited-state keto form may further convert into the triplet-excited-state keto form, which can either return to the ground state and eventually regenerate the original enol or react with nearby molecules to produce degradation products,[2,3] resulting in a loss of UVA protection.

The photostability of AVO primarily depends on the microenvironment in which it resides within a formulation. To optimize the performance of AVO, at least three key ingredients should be considered:

(1) The oil phase (solvents, emollients, and UV absorbers), as the polarity or dielectric constant plays a major role in electron-transfer processes after photon absorption and relaxation.[3–9]

(2) Other UV absorbers incorporated in the oil phase (*e.g.*, octocrylene, octinoxate, and enzacamene), as such molecules can accept triplet energy from the excited-state keto form of AVO and facilitate its return to the ground state.[3,10–18]

(3) Photostabilizers capable of quenching the triplet-excited-state (*e.g.*, diethylhexyl 2,6-naphthalate[19] and polyester-8) or singlet-excited-state (*e.g.*, ethylhexyl methoxycrylene[20]) keto form of AVO.

In addition, novel approaches such as inclusion complex formation with β-cyclodextrin (β-CD) and its derivatives have been reported to improve the photostability of AVO.

Cyclodextrins have various applications in pharmaceutical and cosmetic formulations, including the solubilization and stabilization of active ingredients. Due to its appropriate internal cavity size (inner diameter of 6–6.5 Å),[21] β-CD and its derivatives can encapsulate AVO, thereby providing enhanced photoprotection by reducing photodecomposition and skin permeation. Scalia *et al.* demonstrated that hydroxypropyl-β-CD (HP-β-CD) increases the water solubility and photostability of AVO ($K_{1:1}$ = 2233 M^{-1}; $K_{1:2}$ = 13 M^{-1}).[22] This finding is consistent with the results of Yang *et al.*, who demonstrated that

[a]*James L. Winkle College of Pharmacy, University of Cincinnati, 231 Albert Sabin Way, Cincinnati, OH 45267-0514, USA. E-mail: kumariha@ucmail.uc.edu*
[b]*Helias Catholic High School, 1305 Swifts Hwy, Jefferson City, MO 65109, USA*
[c]*Department of Chemistry, University of Cincinnati, Cincinnati, Ohio 45221, USA*

† Electronic supplementary information (ESI) available. See DOI: https://doi.org/10.1039/d4na00324a

‡ These authors contributed equally.

the incorporation of 30% HP-β-CD ($K_{1:1} = 1580\ M^{-1}$; $K_{1:2} = 16\ M^{-1}$) significantly decreases the photodegradation and skin permeation of AVO.[23] Simeoni *et al.* showed that the effect of sulfobutylether-β-CD (SBE7-β-CD) ($K_{1:1} = 2166.6\ M^{-1}$; $K_{1:2} = 11.9\ M^{-1}$) on reducing accumulated AVO in the epidermis is superior to that of HP-β-CD.[24] Yuan *et al.* reported that (2-hydroxy)propyl-β-CD (2-HP-β-CD) ($K_{1:2} = 14 \times 10^4\ M^{-2}$) improves the water solubility, thermal stability, and photostability of AVO.[25] Lastly, d'Agostino *et al.* demonstrated that β-CD (with an AVO–β-CD ratio of 1 : 2 and no $K_{1:2}$ value reported) enhances the photostability of AVO in the presence of octinoxate.[26]

Yuan *et al.* proposed a mechanism to explain how β-CD and its derivatives improve the photostability of AVO.[25] In this model, one molecule of AVO interacts with two molecules of 2-HP-β-CD, with both the aryl side chains inserted in the cavities through the wider rims, while the diketone moiety remains outside the cavities. The photodegradation of AVO occurs through the triplet excited state of the diketo form. Bond cleavage can occur on either side of the methylene group (within the β-diketone motif), resulting in the formation of phenacyl and benzoyl radicals. However, the presence of 2-HP-β-CD restricts the mobility of these radicals, thereby enhancing cage recombination reactions. Consequently, the photodegradation of AVO complexed with 2-HP-β-CD is reduced.

Furthermore, we hypothesize that the keto–enol equilibrium of AVO plays a crucial role in its photostability upon complexation. The keto–enol equilibrium of β-diketone compounds can be influenced by environmental factors, including incorporation in supramolecular host–guest systems. Studies have demonstrated that β-CD preferentially binds to the enol tautomer of dicarbonyl compounds.[27,28] This preference could explain how β-CD and its derivatives promote the interconversion between the diketo and enol forms of AVO. Among various macrocyclic hosts, cucurbit[7]uril (CB[7]) has been shown to shift the equilibrium toward a keto tautomeric form for coumarin derivatives.[29,30] With a similar cavity size (an inner diameter of 7.3 Å)[31] to that of β-CD, CB[7] is well suited for manipulating the equilibrium between the keto and enol forms of AVO.

In this study, our objective was to establish the impact of macrocyclic compounds (β-CD and CB[7]) on the tautomerization of AVO in aqueous environments. Moreover, we investigated the influence of ethanol as a cosolvent on host–guest complexation and the photostability of AVO. We anticipate that these findings will lay the groundwork for unravelling the mechanisms by which macrocyclic compounds stabilize AVO through keto–enol tautomerism.

Results and discussion

Solution-phase study of AVO and β-CD/CB[7]

For ^{1}H-NMR titration studies in DMSO-d_6, solutions were prepared by dissolving AVO–CB[7] complexes obtained by the kneading method and AVO–β-CD complexes obtained by the solvent evaporation method, as well as pure AVO, CB[7], and β-CD. The NMR signals of the AVO–CB[7] complexes at various molar ratios were characterized by a decrease in protons corresponding to the enol form with a corresponding increase in protons corresponding to the keto form (Fig. 1b). This spectral pattern is evident in the slow exchange regime, when the exchange rate is smaller than the chemical shift difference.[32] The keto–enol equilibrium of AVO is slow enough on the NMR time scale to yield distinct signals for each tautomer. Upon the addition of CB[7], the decrease in signals from the enol tautomer and the simultaneous increase in signals from the keto tautomer suggest that CB[7] complexes with AVO by reducing the enol tautomer (free form) to the keto tautomer (bound form).

For the AVO–β-CD complexes, slight decreases in signals from the enol tautomer were observed upon the addition of β-CD. This behaviour suggests that β-CD influences the keto–enol equilibrium of AVO upon complexation. However, the binding interaction between β-CD and AVO in solution appeared weak,[33] especially compared to that in the AVO–CB[7] complexes. Furthermore, complexation induced shifts in the NMR signals

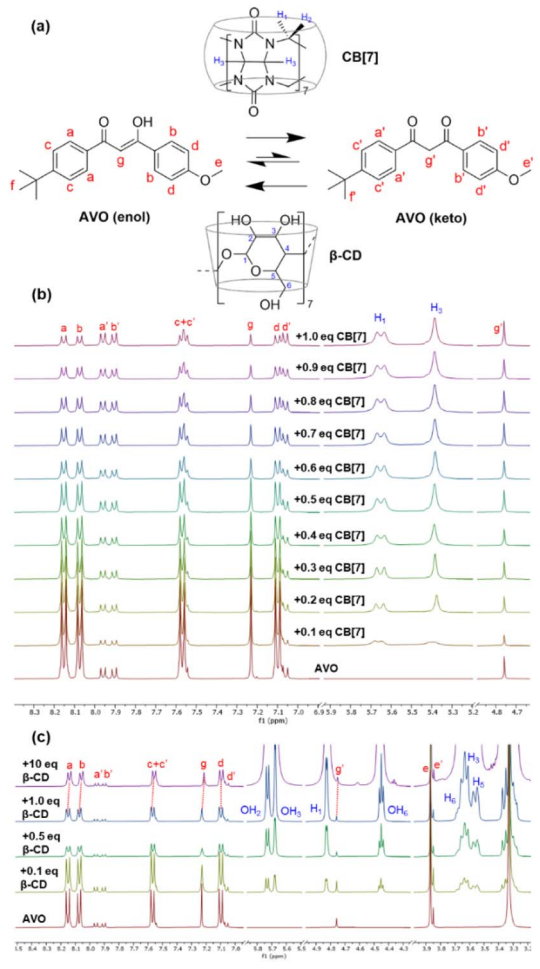

Fig. 1 (a) AVO in keto–enol equilibrium showing protons in red and the shifts in keto–enol equilibrium effected by CB[7] and β-CD (protons of CB[7] and β-CD shown in blue). Stacked plot of the partial ^{1}H-NMR spectra (in DMSO-d_6) of AVO in the absence and presence of (b) CB[7] and (c) β-CD at various molar equivalents.

(Fig. 1c), enabling us to determine the average location of AVO within the β-CD cavity.

All the protons in the dibenzoylmethane moiety of AVO exhibited small upfield shifts (shielding) upon complexation, whereas five protons in β-CD (H-3, H-1, OH-2, OH-3, and OH-6) displayed downfield shifts (deshielding). The location of the β-CD protons is illustrated in Fig. 1a; H-3 is positioned in the cavity near the wider rim, H-1 at the outer interface, OH-2 and OH-3 at the wider rim, and OH-6 at the narrow rim. The shifts in the proton signals for both AVO and β-CD suggest that the dibenzoylmethane moiety of AVO was shallowly inserted and positioned near both the wide and narrow edges of β-CD.

To further explore the possible inclusion between the keto–enol tautomers of AVO with CB[7] and β-CD respectively, We recorded and compared the ^{1}H NMR titration spectra of AVO in the absence and presence of CB[7] and β-CD, respectively. The prominent changes in the NMR spectra of AVO with the inclusion complex are shown in Fig. 2 and 3. Herein, the NMR solvent 90% D_2O/10% EtOD-d_6 mixture containing AVO displays no peaks in the absence of CB[7]. The addition of CB[7] to the same solvent mixture resulted in the appearance of AVO peaks in the spectra and these signals mostly correspond to the keto form of AVO. The subsequent peaks become more prominent with an increase in CB[7] to 6 equivalents (Fig. 2). Similar titrations were performed with β-CD, but no selective NMR signals were observed even upon the addition of up to 12 equivalents of β-CD (Fig. 3). Based on these ^{1}H NMR results, we deduced that there is selective inclusion between the keto–enol tautomers of AVO with CB[7] and β-CD, respectively.

The ^{1}H–^{1}H NOESY NMR technique serves as a compelling method for assessing the relative positions of CB[7] and AVO protons, vital for understanding the structure of inclusion complexes. In order to elucidate and validate the inclusion

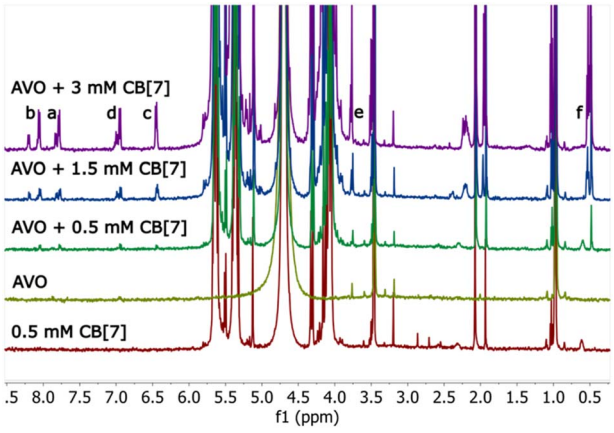

Fig. 2 ^{1}H NMR spectra of AVO in 90% D_2O/10% EtOD-d_6 with increasing amounts of CB[7]. In the apo AVO spectrum (second from the bottom), there are no observable AVO signals. As CB[7] is added, the signals for the aromatic and (f) methyl AVO protons become visible and increase in intensity with increasing CB[7]. AVO peaks are labeled with (a)–(f) according to their corresponding protons on the molecule. In some cases, small minor populations of both AVO and CB[7] peaks are observed, indicating broken symmetries and/or multiple binding orientations.

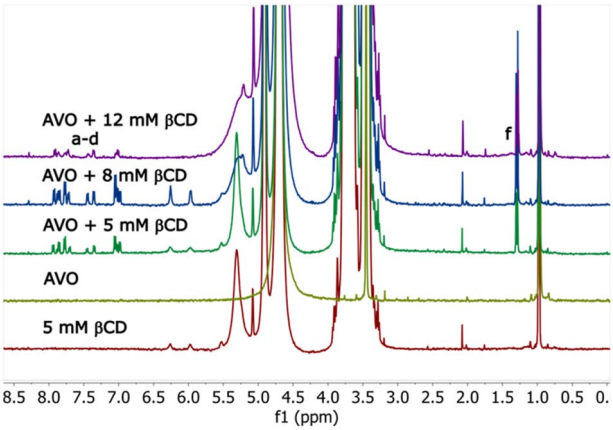

Fig. 3 ^{1}H NMR spectra of AVO in 90% D_2O/10% EtOD-d_6 with increasing amounts of β-CD. In the apo AVO spectrum (second from the bottom), there are no observable AVO signals. As β-CD is added, the signals for the aromatic and (f) methyl AVO protons become visible. Above 8 mM β-CD, the AVO peaks drop in intensity. Aromatic AVO peaks corresponding to protons (a)–(d) were not assigned. In some cases, multiple populations of both AVO and β-CD peaks are observed, indicating broken symmetries and/or multiple binding orientations.

structure of AVO within the CB[7] cavity, a ^{1}H–^{1}H NOESY analysis was conducted in solution, employing a 1 : 6 ratio of AVO to CB[7] in a solvent mixture of 90% D_2O and 10% EtOD-d_1. The highlighted cross-peaks observed between AVO (H_b, H_a, H_d, H_c, and H_e) and the H-1, H-2, and H-3 protons of CB[7] indicate the penetration of AVO into the CB[7] cavity *via* its rims, positioning the AVO moiety towards the interior of the CB[7] cavity (Fig. S2†). However, no cross peaks were observed while performing the ^{1}H–^{1}H NOESY analysis for AVO to β-CD in a solvent mixture of 90% D_2O and 10% EtOD-d_6 due to low sensitivity (Fig. S3†).

The DOSY NMR experiments of AVO : CB[7] and AVO : β-CD in 90% D_2O/10% EtOD-d_1 were carried out to further confirm the presence of inclusion complexes. We observe a single diffusion constant for both complexes around −9.64 (units are log (m^2 s^{-1})) passing through AVO aromatic peaks and host peaks confirming the formation of inclusion products in both cases (Fig. S4 and S5†). In the case of AVO : CB[7] (Fig. S4†), it corresponds to a diffusion rate of $10^{-9.64}$ or 2.29×10^{-10} m^2 s^{-1} and in the case of AVO : β-CD (Fig. S5†), it corresponds to a diffusion rate of $10^{-9.63}$ or 2.34×10^{-10} m^2 s^{-1}. Notably the diffusion coefficient values for two complexes are similar due to the similar molecular weights of hosts (CB[7]: 1163 g mol; β-CD: 1135 g mol^{-1}).

The UV-Vis titration spectra of AVO in the presence of CB[7] and β-CD are shown in Fig. 4 to illustrate the interactions of AVO with CB[7] and β-CD. AVO exhibited two absorbance bands in ethanol/water. The first band at λ_{max} = 270 nm can be attributed to a n–π* transition involving the n-electrons of the carbonyl group in the keto tautomer. The second band at λ_{max} = 360 nm corresponds to the π–π* transition of the C=C enolic form. Upon the addition of CB[7], the absorbance at λ_{max} = 270 nm increased, indicating a shift in the equilibrium toward

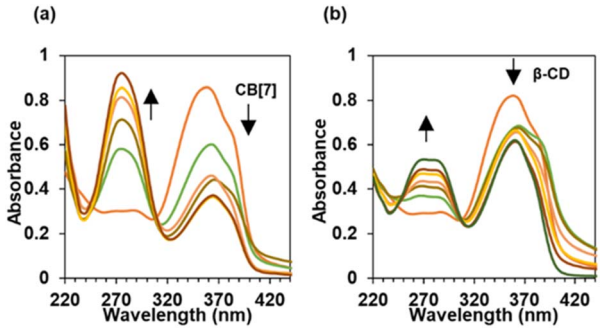

Fig. 4 UV-Vis titration spectra of (a) AVO (0.04 mM) in the presence of CB[7] (0–2 mM) in 10% ethanol and (b) AVO (0.04 mM) in the presence of β-CD (0–4 mM) in 10% ethanol.

the keto tautomer. When β-CD was added, shifts in the tautomeric equilibrium were detected for the AVO–β-CD complexes in hydro-alcoholic solutions with low ethanol contents (10% in Fig. 4b and 20% in Fig. S6†), consistent with the ^{1}H-NMR titration results. Moreover, a hyperchromic effect was observed in higher ethanol contents (30% and 40%, Fig. S6†), indicating an increase in the solubility of AVO in the ethanol/water solution due to complex formation.

The stoichiometric ratio and association constant (K_a) of the individual complexes in ethanol/water solutions were determined using the Benesi–Hildebrand method[34–36] (see the ESI†). The plots of [AVO]/($A - A_0$) as a function of 1/[H] in Fig. S8† exhibit linear relationships, indicating 1 : 1 stoichiometry for both the AVO–β-CD and AVO–CB[7] complexes at all concentrations in ethanol/water solutions. The K_a values were calculated from the intercept and slope values (Table S1†), as shown in Table 1. K_a values of less than 500 M^{-1} were obtained for the AVO–β-CD complexes, suggesting a weak bond strength, whereas K_a values of 1000–5000 M^{-1} were determined for the AVO–CB[7] complexes, indicating a moderate binding.[33]

Solid-state study of AVO and β-CD/CB[7]

After drying, a white powder was obtained for AVO–β-CD and a yellowish powder for AVO–CB[7]. The color of the AVO–CB[7] complex changed from pinkish to yellowish as the mole ratio of CB[7] increased.

The overlaid FTIR spectra of AVO, CB[7], and the AVO–CB[7] complex are presented in Fig. 5a. AVO exhibits characteristic peaks at 2960, 1583, 1256, and 1021 cm^{-1} corresponding to CH_3 stretching, C=O stretching, C(sp^2)–O stretching, and C(sp^3)–O stretching, respectively. In the case of the CB[7] powder, the peak at 1712 cm^{-1} is assigned to C=O stretching. From the spectrum of the AVO–CB[7] complex, the position of the CB[7] peak (C=O stretching) is shifted from 1712 to 1731 cm^{-1}, indicating complex formation. This shift in the C=O stretching band implies an interaction between CB[7] and AVO in the carbonyl portal region. However, specifying the part of AVO that interacts with CB[7] is challenging, as the bands corresponding to AVO only exhibit a decrease in intensity without shifting.

The overlaid FTIR spectra of AVO, β-CD, and the AVO–β-CD complex are shown in Fig. 5b. The interpretation of the β-CD spectrum is complicated because of the absence of distinct characteristic bands. However, for the bands associated with AVO, slight shifts in the peak position from 1583 to 1603 cm^{-1}, accompanied by changes in the band shape, and from 1256 to 1264 cm^{-1}, accompanied by a decrease in intensity, were observed for the AVO–β-CD complex. These spectral changes suggest the occurrence of complexation.

Computational results

Classical MD and electronic structure calculations were used to explore possible interactions between AVO and β-CD or CB[7] in the presence of water or water/ethanol as a solvent. To track these interactions, the radii of the β-CD and CB[7] hosts, the distance between the host center of mass (COM) and the central carbon of *t*-Bu ($C_{t\text{-Bu}}$), the distance between the host COM and the MeO carbon (C_{MeO}), and the distance between $C_{t\text{-Bu}}$ and C_{MeO} were recorded for production runs and all other NPT trajectories (Tables S2–S4†). The host radii for β-CD were obtained by determining the COM of the molecule using the heavy atoms in the glucose-based subunits and then measuring the distance to the COM of individual glucose-based subunits; the same process was used for the heavy atoms in the glycoluril subunits of CB[7]. The host$_{COM}$–AVO$_{COM}$ values were determined using the COM of all the atoms in the complexes.

Several distances were used as metrics to better understand the simulation results. For all the NPT simulations, regardless

Table 1 Association constant (K_a) values (M^{-1}) for the 1 : 1 stoichiometry of AVO–β-CD and AVO–CB[7] complexes at varied ethanol/water concentrations obtained by the Benesi–Hildebrand method

Complexes	% Ethanol	$K_a \pm$ SD[a]	R^2
AVO–β-CD	10	140 ± 20	0.9970
	20	90 ± 20	0.9946
	30	470 ± 50	0.9847
	40	310 ± 20	0.9924
AVO–CB[7]	10	1360 ± 120	0.9876
	20	1400 ± 230	0.9566

[a] SD is the error of the K_a calculated as:[37] $SD = K_a \times \sqrt{\left(\frac{\text{standard error of slope}}{\text{slope}}\right)^2 + \left(\frac{\text{standard error of intercept}}{\text{intercept}}\right)^2}$.

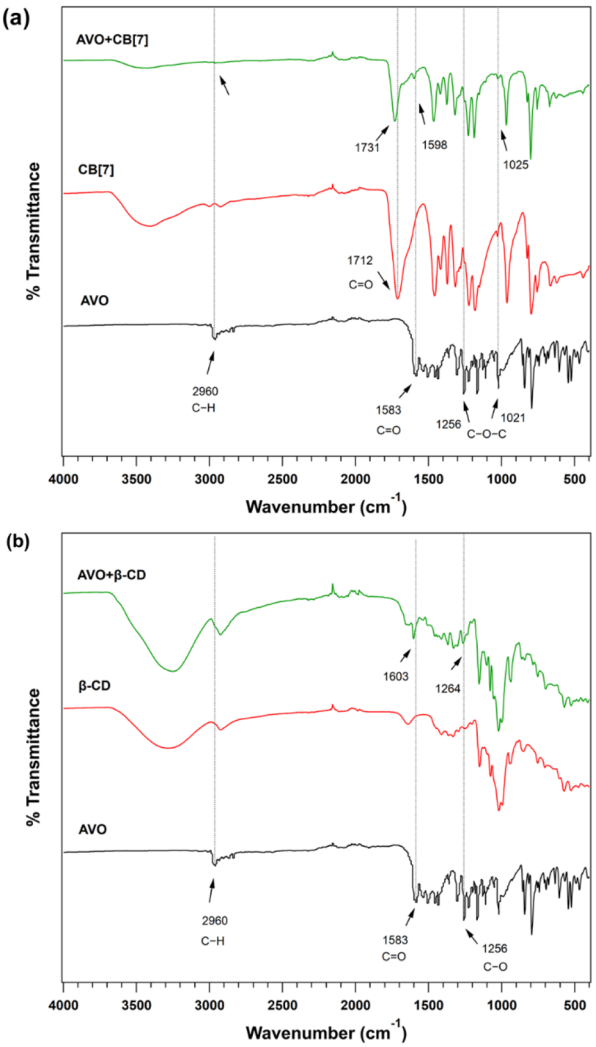

Fig. 5 FTIR spectra of (a) (top to bottom) the AVO–CB[7] complex (1 : 1) prepared by the kneading method, CB[7], and AVO; (b) (top to bottom) the AVO–β-CD complex (1 : 1) prepared by the solvent evaporation method, β-CD, and AVO.

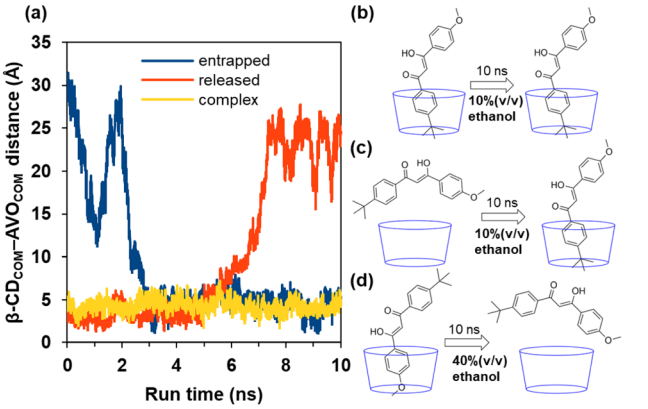

Fig. 6 (a) Plot of the host$_{COM}$–AVO$_{COM}$ distance against the run time (ns) for three different AVO–β-CD systems: complex or (b) AVO–β-CD complex with a starting orientation of *t*-Bu inserted within the narrow rim in 10% ethanol, showing the typical behaviour of a host–guest complex with minimal fluctuation in the host–guest distance (remains complexed); entrapped or (c) AVO–β-CD complex with a starting orientation of AVO above β-CD in 10% ethanol, demonstrating guest entrapment; released or (d) AVO–β-CD complex with a starting orientation of MeO inserted within the narrow rim in 40% ethanol, demonstrating the departure of the guest from the host. These data demonstrate that sterics can contribute to the continual entrapment of AVO, regardless of the host, but favourable interactions and a lower ethanol content can also lead to entrapment. Note that water and ethanol molecules were omitted for clarity.

of the solvent mixture, the average host radii varied by less than 0.02 Å, demonstrating the robust framework of the hosts, and the β-CD radius was ~1 Å greater than that of CB[7] (Tables S2–S4†). The distance measured from host$_{COM}$ to C$_{t\text{-Bu}}$ and C$_{MeO}$ varied among the systems depending on the freedom of the AVO molecule. Notably, the systems with an entrapped AVO molecule (*e.g.*, the AVO–CB[7] complex with *t*-Bu within the CB[7] cavity) exhibited much less fluctuation in the host$_{COM}$–C$_{t\text{-Bu}}$ distance compared with the host$_{COM}$–C$_{MeO}$ distance. When entrapped, AVO tended to remain elongated, as evidenced by the longer C$_{MeO}$–C$_{t\text{-Bu}}$ distances; however, when AVO was not within a host, fewer torsional restrictions resulted in smaller C$_{t\text{-Bu}}$–C$_{MeO}$ distances.

For the initial orientations with AVO interacting with the host molecule, AVO remained within the cavity, except for the AVO–β-CD complex in 40% ethanol when the MeO end was entrapped. In this production run, AVO remained within β-CD for approximately 6 ns and then left the host and interacted with the side of the host for ~1 ns before moving away from the host (Fig. 6). This specific orientation could have non-conventional OH–π interactions between β-CD and the phenyl group of AVO, which would serve as an anchor as the solvent begins to interact with AVO until all interactions are disrupted. This case is consistent with experimental evidence for a smaller complexation number as the fraction of ethanol increases.

Interestingly, in an initial NPT simulation of AVO–β-CD in H_2O, the distance between AVO$_{COM}$ and β-CD$_{COM}$ decreased from ~25 to ~8 Å until AVO interacted with the side of β-CD (Table S3†). This behaviour was only observed for the AVO–β-CD complex in 20% ethanol, where AVO was above β-CD. In fact, after approximately 2.5 ns, AVO began to interact with the wide rim of β-CD before becoming encapsulated. This guest migration behaviour combined with several torsions of the guest molecule led to unexpected data compared with that at other ethanol concentrations (Table S2†). Upon further analysis of this simulation, the host$_{COM}$–AVO$_{COM}$ distance was found to be within the average determined for the other encapsulated simulations (~5 Å) for 40% of the simulation.

Our quantum chemical studies identified a number of equilibrium structures for the AVO–CB[7] and AVO–systems with the orientations discussed in the Computational results section. Compared with the MD results, the radii of the β-CD and CB[7] hosts are ~0.03 and 0.3 Å too large, respectively (Table S5†), but similar orientations within the host cavity are observed. When comparing the host–guest configurations, the Δ*H* and Δ*G* values exhibit some variation in terms of relative stability depending on the SPE method employed (*e.g.*, several

AVO–β-CD complexes are more stable (<15 kJ mol^{-1}) in the gas phase than when accounting for implicit solvent (Tables S6 and S7†)). Typically, larger differences in relative stability are observed in the ωB97X-D data than in the M06-2X data. In general, the inclusion of implicit solvents has a much larger contribution to the stability of the CB[7] complexes (differences of ∼30 kJ mol^{-1}) than the β-CD complexes (differences of 15 kJ mol^{-1} except when AVO is oriented to the side of β-CD). Notably, the orientations with AVO interacting with the internal cavity (*t*-Bu or MeO within the cavity) are more stable than those with AVO interacting with the outside of the cavity.

The dissociation of the AVO–CB[7] and AVO–β-CD complexes is most favourable when AVO is oriented such that the *t*-Bu group is within the host cavity. Although both host–guest complexes are more favorable than the isolated host and guest, the Δ*H* and Δ*G* for the dissociation reactions are more favourable for AVO–CB[7] than for AVO–β-CD (eqn (S2) (S3) and Table S7†). For the dissociation reactions, the Δ*H* and Δ*G* values calculated using ωB97X-D/6-311+G(d,p) are 50–54 kJ mol^{-1} higher than those obtained using M06-2X/6-311+G(d,P). When considering gas-phase and implicit solvent effects, the AVO–CB[7] complex exhibited higher Δ*H* (19–27 kJ mol^{-1}) and Δ*G* (0.5–9 kJ mol^{-1}) values than the AVO–β-CD complex, supporting the experimental observation of a stronger interaction between AVO and CB[7]. One possible reason for the lower dissociation energetics of the β-CD complex could be the presence of an extensive hydrogen-bonded network within the isolated β-CD complex, whereas a similar structure cannot be formed by isolated CB[7]. At a given level of theory, the host–guest complex was more thermodynamically favourable with the inclusion of solvent effects. H_2O as the solvent led to dissociation energetics within 5 kJ mol^{-1} of the gas-phase values, whereas ethanol led to a decrease of 6–10 kJ mol^{-1} relative to the gas-phase values.

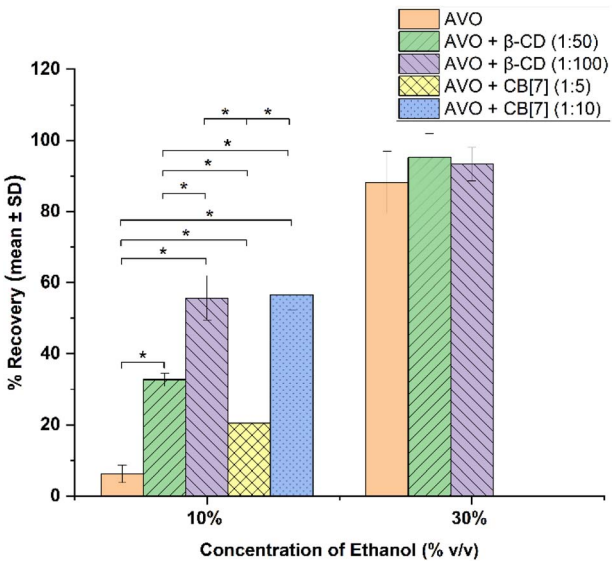

Fig. 7 Effect of the host (β-CD or CB[7]) and ethanol on the photostability of AVO after 60 min irradiation, expressed as % recovery. A "*" denotes a significant difference ($\alpha = 0.05$) between two groups, and the range of the error bar is the mean ± standard deviation ($n = 3$).

In the presence of ethanol, the Δ*G* values determined using M06-2X/6-311+G(d,p) suggested nearly thermoneutral dissociation, consistent with the experimental finding that higher ethanol concentrations can affect the formation of the host–guest complex.

Photostability results

The UV spectra of AVO alone in 10% and 30% ethanol/water, AVO–β-CD (1 : 100 and 1 : 50 molar ratios) in 10% and 30% ethanol/water, and AVO–CB[7] (1 : 10 and 1 : 5 molar ratios) in 10% ethanol/water before and after irradiation for 60 min are overlaid in Fig. S10.† The reduction in absorbance after irradiation indicates a decrease in the concentration of AVO, consistent with the quantitative HPLC-UV results, as shown in Fig. 7 and Table S8.† AVO exhibited poor photostability in 10% ethanol/water, with a recovery of 6 ± 2%, whereas good stability was observed in 30% ethanol/water, with a recovery of 88 ± 9%, suggesting that ethanol improves the photostability of AVO,[38] possibly because ethanol shortens the triplet excited state lifetime of AVO.[10]

Upon complexation with β-CD or CB[7], AVO showed superior photostability compared to AVO alone in 10% ethanol/water. At molar ratios of 1 : 100 for AVO–β-CD and 1 : 10 for AVO–CB[7] in 10% ethanol/water, higher recoveries of 56 ± 6% and 57 ± 4%, respectively, were obtained. According to the solution-phase results, β-CD and CB[7] show similar complexation behaviour with AVO in 10% ethanol/water. Both β-CD and CB[7] form complexes with AVO by converting the enol tautomer to the keto tautomer, which suggests that the bound form (keto form) is photostabilized by β-CD and CB[7]. The percent recovery for the two solutions was expected to be similar. As the K_a value for the AVO–β-CD complex was approximately 1/10 of that for the AVO–CB[7] complex, AVO–β-CD at a molar ratio of 1 : 100 and AVO–CB[7] at a molar ratio of 1 : 10 should provide similar values for % bound AVO. As shown in Table S9,† the calculated concentrations of % bound AVO in both solutions are 99%.

The impact of β-CD and CB[7] concentrations on photostabilization was investigated for AVO–β-CD at a molar ratio of 1 : 50 and AVO–CB[7] at a molar ratio of 1 : 5 in 10% ethanol/water, which have % bound AVO values of 98% and 97%, respectively. The AVO–β-CD and AVO–CB[7] complexes achieved higher recoveries (33 ± 2% and 20 ± 2%, respectively) than AVO alone. Notably, a lower concentration of the host yielded a lower efficiency of guest protection, although the % bound AVO value decreased by only approximately 1%. Surprisingly, the recoveries for 1 : 5 AVO–CB[7] and 1 : 50 AVO–β-CD were statistically different, emphasizing that the host concentration and the optimum molar ratio between the guest and host have a major impact on the photostability of AVO in environments with low ethanol concentrations.

The effect of ethanol on complexation and photostability was tested using AVO–β-CD at molar ratios of 1 : 100 and 1 : 50 in 30% ethanol/water, which have % bound AVO values of almost 100% and 99%, respectively. According to the solution-phase studies in 30% ethanol, β-CD forms complexes with both the

keto and enol forms by increasing their water solubility, but it is unclear whether β-CD shifts the keto–enol equilibrium of AVO. For the 1 : 100 and 1 : 50 complexes in solution, similar AVO recoveries were obtained (93 ± 5% and 95 ± 7%, respectively), which were higher than that of AVO alone (88 ± 9%, % recovery), despite there being no statistically significant differences among the three solutions. These observations suggest that in environments with high ethanol concentrations, ethanol prominently influences the photostability of AVO and lower β-CD concentrations are sufficient for enhancing photostabilization.

ESI-MS experiments were conducted to confirm that AVO–β-CD and AVO–CB[7] remained complexed under irradiation. The ESI-MS spectra of AVO–β-CD (1 : 1) and AVO–CB[7] (1 : 1) after irradiation for 0, 30, and 60 min are overlaid in Fig. S11, S12 and Table S10.† Under the ESI-MS conditions (acidic environment), AVO was complexed with β-CD or CB[7], but the complex concentrations decreased as a function of irradiation time. This behavior confirms that the keto form of AVO is preferentially complexed and is stabilized by β-CD or CB[7].

Conclusions

We have shown that the formation of AVO complexes was affected by the type of macrocycle (CB[7] or β-CD) and the concentration of ethanol (cosolvent) in the aqueous environment (10%, 20%, 30%, and 40% ethanol). In solution-phase studies, CB[7] and β-CD formed 1 : 1 host–guest complexes with AVO by converting the enol tautomer to the keto tautomer at lower ethanol concentrations (10% and 20%), whereas at 30% and 40% ethanol, β-CD formed 1 : 1 host–guest complexes with AVO by increasing the water solubility of both the keto and enol forms. The K_a value for AVO–CB[7] was 1360 M^{-1} and 1400 M^{-1} in 10% and 20% ethanol, respectively, whereas the highest K_a value for AVO–β-CD was 470 M^{-1} in 30% ethanol, possibly due to differences in solubility behaviour. Increasing the ethanol concentration to 40% resulted in a lower K_a value (310 M^{-1}) for AVO–β-CD, which was attributed to ethanol disrupting the interactions between AVO and β-CD or competing with AVO. In solid-state studies, the formation of AVO complexes was confirmed by FTIR spectroscopy. Computational studies provided further insights into the structural properties and energetics of the AVO–CB[7] and AVO–β-CD complexes. MD simulations in the presence of explicit solvent showed structural agreement with gas-phase DFT calculations. Higher-level SPE calculations with the ωB97X-D method revealed that the host–guest complex was favoured over isolated AVO and β-CD or CB[7] molecules by 95–125 kJ mol^{-1}, depending on the presence of implicit solvent. Upon UV irradiation, the keto form of AVO was photostabilized by complexation with CB[7] over β-CD in an aqueous environment (10% ethanol/water), with the degree of stabilization depending on the host concentration and K_a value of the complex. This study has demonstrated that selecting CB[7] for complexation with β-diketone-containing molecules, including AVO, is an effective strategy for intentionally shifting the keto–enol equilibrium towards the keto form.

Data availability

The data supporting this article have been included as part of the ESI.†

Author contributions

JP designed and conducted all experiments and wrote the manuscript; CMM, KCK, and MLC performed theoretical calculation and wrote the theory portion of the manuscript; AAD performed the synthesis of macrocycles, formal NMR data analysis, and review and editing of the manuscript, AIG conducted NMR experiments, formal analysis, and review and editing of the manuscript; HK conducted conceptualization, review and editing of the manuscript, and supervision.

Conflicts of interest

There are no conflicts to declare.

Acknowledgements

The authors would like to acknowledge Stephen F. Macha, PhD, of the R. Marshall Wilson Mass Spectrometry Facility for ESI-MS experiments and Necati Kaval, PhD, of the Chemistry Department Facility at the University of Cincinnati for valuable discussions concerning ATR-FTIR data. Calculations were carried out at the Ohio Supercomputer Center, which provides high-performance computing resources.[39] This work was funded by the University of Cincinnati (HK) and AFOSR Grant # FA95502310413 (HK).

Notes and references

1 A. Medici, G. Luongo, G. Di Fabio and A. Zarrelli, Environmental Fate of Organic Sunscreens during Water Disinfection Processes: The Formation of Degradation By-Products and Their Toxicological Profiles, *Molecules*, 2022, **27**, 4467.
2 J. Kockler, S. Robertson, M. Oelgemoller, M. Davies, B. Bowden, H. G. Brittain and B. D. Glass, Butyl methoxy dibenzoylmethane, *Profiles Drug Subst Excip Relat Methodol*, 2013, vol. 38, pp. 87–111.
3 C. A. Bonda, The Photostability of Organic Sunscreen Actives: A Review, in *Sunscreens*, ed. N. A. Shaath, Taylor & Francis, Boca Raton, 2005, pp. 321–349.
4 J. J. Vallejo, M. Mesa and C. Gallardo, Evaluation of The Avobenzone Photostability in Solvents Used in Cosmetic Formulations, *Vitae*, 2011, **18**, 63–71.
5 G. J. Mturi and B. S. Martincigh, Photostability of the sunscreening agent 4- tert-butyl-4′-methoxydibenzoylmethane (avobenzone) in solvents of different polarity and proticity, *J. Photochem. Photobiol., A*, 2008, **200**, 410–420.
6 S. P. Huong, E. Rocher, J.-D. Fourneron, L. Charles, V. Monnier, H. Bun and V. Andrieu, Photoreactivity of the sunscreen butylmethoxydibenzoylmethane (DBM) under

various experimental conditions, *J. Photochem. Photobiol., A*, 2008, **196**, 106–112.
7 S. Durango, S. Castañeda, J. Vallejo and C. Gallardo, Solvent effect on photostability of butyl methoxy di benzoyl methane formulated in solution and emulsion, *Int. J. Pharm. Sci.*, 2015, **7**, 181–186.
8 E. R. Barthel, I. B. Martini and B. J. Schwartz, How Does the Solvent Control Electron Transfer? Experimental and Theoretical Studies of the Simplest Charge Transfer Reaction, *J. Phys. Chem. B*, 2001, **105**, 12230–12241.
9 M. Maroncelli, J. Macinnis and G. R. Fleming, Polar solvent dynamics and electron-transfer reactions, *Science*, 1989, **243**, 1674–1681.
10 A. Cantrell, D. J. McGarvey and T. G. Truscott, Chapter 26 - Photochemical and photophysical properties of sunscreens, *Comprehensive Series in Photosciences*, ed. P. U. Giacomoni, Elsevier, 2001, vol. 3, pp 495–519.
11 A. Kikuchi, N. Oguchi-Fujiyama, K. Miyazawa and M. Yagi, Triplet-Triplet Energy Transfer from a UV-A Absorber Butylmethoxydibenzoylmethane to UV-B Absorbers, *Photochem. Photobiol.*, 2014, **90**, 511–516.
12 A. Kikuchi, Y. Hata, R. Kumasaka, Y. Nanbu and M. Yagi, Photoexcited Singlet and Triplet States of a UV Absorber Ethylhexyl Methoxycrylene, *Photochem. Photobiol.*, 2013, **89**, 523–528.
13 S. Matsumoto, R. Kumasaka, M. Yagi and A. Kikuchi, Triplet–triplet energy transfer between UV absorbers in solutions at room temperature, *J. Photochem. Photobiol., A*, 2017, **346**, 396–400.
14 V. Lhiaubet-Vallet, M. Marin, O. Jimenez, O. Gorchs, C. Trullas and M. A. Miranda, Filter-filter interactions. Photostabilization, triplet quenching and reactivity with singlet oxygen, *Photochem. Photobiol. Sci.*, 2010, **9**, 552–558.
15 R. M. Sayre, J. C. Dowdy, A. J. Gerwig, W. J. Shields and R. V. Lloyd, Unexpected Photolysis of the Sunscreen Octinoxate in the Presence of the Sunscreen Avobenzone, *Photochem. Photobiol.*, 2005, **81**, 452–456.
16 A. Kikuchi and M. Yagi, Direct observation of the intermolecular triplet–triplet energy transfer from UV-A absorber 4-*tert*-butyl-4′-methoxydibenzoylmethane to UV-B absorber octyl methoxycinnamate, *Chem. Phys. Lett.*, 2011, **513**, 63–66.
17 H. Gonzenbach, T. J. Hill and T. G. Truscott, The Triplet Energy Levels of UVA and UVB Sunscreens, *J. Photochem. Photobiol., B*, 1992, **16**, 377–379.
18 B. Herzog, J. Giesinger and V. Settels, Insights into the stabilization of photolabile UV-absorbers in sunscreens, *Photochem. Photobiol. Sci.*, 2020, **19**, 1636–1649.
19 R. Shimizu, M. Yagi, N. Oguchi-Fujiyama, K. Miyazawa and A. Kikuchi, Photophysical properties of diethylhexyl 2,6-naphthalate (Corapan TQ), a photostabilizer for sunscreens, *Photochem. Photobiol. Sci.*, 2018, **17**, 1206–1212.
20 S. Mandar, P. Wulandari, V. F. Savitri, H. Aziz, R. Suhaili and Y. Rahmawati, Photostability of avobenzone in a commercial sunscreen SPF 50 with the addition of quencher upon sun exposure, *Int. J. Sci. Rep.*, 2023, **9**, 202–209.
21 G. Crini and L. Aleya, Cyclodextrin applications in pharmacy, biology, medicine, and environment, *Environ. Sci. Pollut. Res.*, 2022, **29**, 167–170.
22 S. Scalia, S. Villani, A. Scatturin, M. A. Vandelli and F. Forni, Complexation of the sunscreen agent, butyl-methoxydibenzoylmethane, with hydroxypropyl-β-cyclodextrin, *Int. J. Pharm.*, 1998, **175**, 205–213.
23 J. Yang, C. J. Wiley, D. A. Godwin and L. A. Felton, Influence of hydroxypropyl-beta-cyclodextrin on transdermal penetration and photostability of avobenzone, *Eur. J. Pharm. Biopharm.*, 2008, **69**, 605–612.
24 S. Simeoni, S. Scalia and H. A. E. Benson, Influence of cyclodextrins on in vitro human skin absorption of the sunscreen, butyl-methoxydibenzoylmethane, *Int. J. Pharm.*, 2004, **280**, 163–171.
25 L. Yuan, S. Li, D. Huo, W. Zhou, X. Wang, D. Bai and J. Hu, Studies on the preparation and photostability of avobenzone and (2-hydroxy)propyl-β-cyclodextrin inclusion complex, *J. Photochem. Photobiol., A*, 2019, **369**, 174–180.
26 S. D'Agostino, A. Azzali, L. Casali, P. Taddei and F. Grepioni, Environmentally Friendly Sunscreens: Mechanochemical Synthesis and Characterization of β-CD Inclusion Complexes of Avobenzone and Octinoxate with Improved Photostability, *ACS Sustainable Chem. Eng.*, 2020, **8**, 13215–13225.
27 E. Iglesias, Inclusion Complexes of β-Cyclodextrin with Keto/Enol Tautomers of 2-Acetyl-1-tetralone. A Comparative Study, *J. Inclusion Phenom. Macrocyclic Chem.*, 2005, **52**, 55–62.
28 E. Iglesias, V. Ojea-Cao, L. García-Rio and J. R. Leis, Effects of β-Cyclodextrin on the Keto−Enol Equilibrium of Benzoylacetone and on Enol Reactivity, *J. Org. Chem.*, 1999, **64**, 3954–3963.
29 M. E. Aliaga, L. García-Río, A. Numi, A. Rodríguez, S. Arancibia-Opazo, A. Fierro and A. Cañete, Controlled keto-enol tautomerism of coumarin containing β-ketodithioester by its encapsulation in cucurbit[7]uril, *New J. Chem.*, 2017, **41**, 15574–15580.
30 R. H. Alzard, M. S. Bufaroosha, N. Al-Shamsi, A. Sohail, N. Al-Dubaili, A. A. Salem, I. M. Abdou and N. Saleh, Solubilization of Pyridone-Based Fluorescent Tag by Complexation in Cucurbit[7]uril, *ACS Omega*, 2019, **4**, 953–960.
31 M. J. Webber and R. Langer, Drug delivery by supramolecular design, *Chem. Soc. Rev.*, 2017, **46**, 66–662.
32 A. U. Rahman and M. I. Choudhary, *Applications of NMR Spectroscopy*, 2015, vol. 1.
33 A. I. Takahashi, F. J. B. Veiga and H. G. Ferraz, Literature review of cyclodextrins inclusion complexes characterization - Part I: phase solubility diagram, dissolution and scanning electron microscopy, *Int. J. Pharm. Sci. Rev. Res.*, 2012, **12**, 1–6.
34 O. Exner, Calculating equilibrium constants from spectral data: reliability of the Benesi-Hildebrand method and its modifications, *Chemom. Intell. Lab. Syst.*, 1997, **39**, 85–93.
35 I. D. Kuntz Jr, F. P. Gasparro, M. D. Johnston Jr and R. P. Taylor, Molecular interactions and the Benesi-Hildebrand equation, *J. Am. Chem. Soc.*, 1968, **90**, 4778–4781.

36 R. Wang and Z. Yu, Validity and Reliability of Benesi-Hildebrand Method, *Acta Phys.-Chim. Sin.*, 2007, **23**, 1353–1359.
37 G. Chalumot, C. Yao, V. Pino and J. L. Anderson, Determining the stoichiometry and binding constants of inclusion complexes formed between aromatic compounds and β-cyclodextrin by solid-phase microextraction coupled to high-performance liquid chromatography, *J. Chromatogr. A*, 2009, **1216**, 5242–5248.
38 M. Cowden, A. L. Whittock, E. L. Holt, V. G. Stavros and M. Wills, Synthesis and characterisation of novel composite sunscreens containing both avobenzone and octocrylene motifs, *RSC Adv.*, 2023, **13**, 17017–17027.
39 Ohio Supercomputer Center, *Ohio Supercomputer Center*, 1987, **http://osc.edu/ark:/19495/f5s1ph73**.